

Thickness dependence of spin Peltier effect visualized by thermal imaging technique

Shunsuke Daimon,^{1,2,3,*} Ken-ichi Uchida,^{1,4,5,6,†} Naomi

Ujiie,⁷ Yasuyuki Hattori,⁷ Rei Tsuboi,¹ and Eiji Saitoh^{1,2,3,6,8}

¹*Institute for Materials Research, Tohoku University, Sendai 980-8577, Japan*

²*Advanced Institute for Materials Research,
Tohoku University, Sendai 980-8577, Japan*

³*Department of Applied Physics, The University of Tokyo, Tokyo 113-8656, Japan*

⁴*National Institute for Materials Science, Tsukuba 305-0047, Japan*

⁵*Department of Mechanical Engineering,
The University of Tokyo, Tokyo 113-8656, Japan*

⁶*Center for Spintronics Research Network,
Tohoku University, Sendai 980-8577, Japan*

⁷*ALPS ALPINE CO., LTD., Tokyo 145-8501, Japan*

⁸*Advanced Science Research Center, Japan Atomic Energy Agency, Tokai 319-1195, Japan*

Abstract

Magnon propagation length in a ferrimagnetic insulator yttrium iron garnet (YIG) has been investigated by measuring and analyzing the YIG-thickness t_{YIG} dependence of the spin Peltier effect (SPE) in a Pt/YIG junction system. By means of the lock-in thermography technique, we measured the spatial distribution of the SPE-induced temperature modulation in the Pt/YIG system with the t_{YIG} gradation, allowing us to obtain the accurate t_{YIG} dependence of SPE with high t_{YIG} resolution. Based on the t_{YIG} dependence of SPE, we verified the applicability of several phenomenological models to estimate the magnon diffusion length in YIG.

Interconversion between spin and heat currents has been extensively studied in the field of spin caloritronics [1, 2]. One of the spin-caloritronic phenomena is the spin Seebeck effect (SSE) [3], which generates a spin current as a result of a heat current in metal/magnetic-insulator junction systems. The Onsager reciprocal of SSE is the spin Peltier effect (SPE) [4–11]. A typical system used for studying SPE and SSE is paramagnetic metal Pt/ferrimagnetic insulator yttrium iron garnet (YIG) junction systems [3–5, 7, 12–15], where the spin and heat currents are carried by electron spins in Pt and magnons in YIG [16–19].

SPE and SSE are characterized by their length scale including the magnon-spin diffusion length l_m and the magnon-phonon thermalization length l_{mp} in YIG [18, 20, 21]. These length parameters have been investigated by measuring discrete YIG-thickness t_{YIG} dependence of SPE and SSE in several Pt/YIG junction systems with different t_{YIG} [7, 13, 14, 21, 22]. However, different junctions may have different magnetic properties, surface roughness, crystallinity, and interface condition. These variations make it hard to analyze the fine t_{YIG} dependence and obtain correct values of the length parameters.

In this letter, we measured the t_{YIG} dependence of SPE by using a single Pt/YIG system with a t_{YIG} gradient (∇t_{YIG}). Since SPE induces temperature change reflecting the local t_{YIG} value, we can extract the t_{YIG} dependence of SPE from a temperature distribution. The spatial distribution of the SPE-induced temperature change was visualized by means of the lock-in thermography (LIT) [5]. The LIT method allows us to obtain the accurate t_{YIG} dependence of SPE with high t_{YIG} resolution. By means of the thermoelectric imaging technique based on laser heating [23], we also measured the t_{YIG} dependence of SSE in a single Pt/YIG system, which shows the same behavior as that of SPE. By analyzing the measured t_{YIG} dependence of SPE and using phenomenological models, we estimated l_m and determined the upper limit of l_{mp} for YIG.

The sample used for measuring SPE consists of a Pt film and an YIG film with ∇t_{YIG} [Fig. 1(a),(d)]. ∇t_{YIG} was introduced by obliquely polishing a single-crystalline YIG (111) film grown by a liquid phase epitaxy method on a single-crystalline $Gd_3Fe_5O_{12}$ (GGG) (111) substrate. The obtained ∇t_{YIG} is almost uniform in the measurement range, which was observed to be $9.2 \mu\text{m}$ per a 1 mm lateral length by a cross-sectional scanning electron microscopy [Fig. 1(f)]. After the polishing, a U-shaped Pt film with a thickness of 5 nm and width of 0.5 mm was sputtered on the surface of the YIG film. The longer lines of the U-shaped Pt film were along the ∇t_{YIG} direction. In the microscope image of the sample in Fig. 1(d), the yellow (gray) area above (below) the white dotted line corresponds to the YIG film with ∇t_{YIG} (GGG substrate).

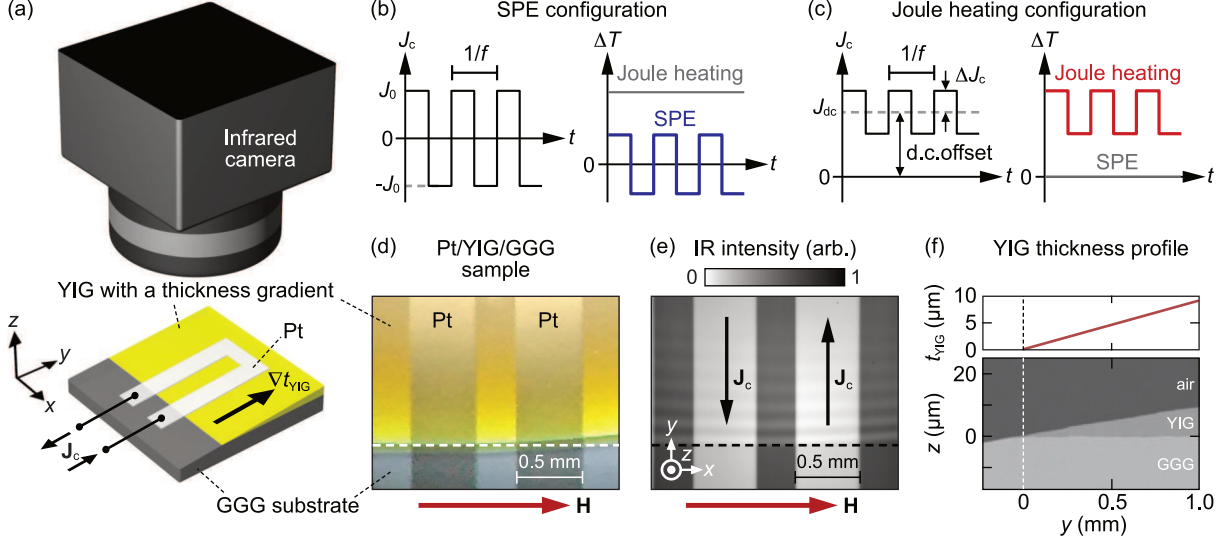


FIG. 1: (a) Schematic of the SPE measurement using a Pt/YIG/GGG sample by means of the lock-in thermography method. A charge current \mathbf{J}_c is applied to the U-shaped Pt film fabricated on the YIG film with a thickness gradient ∇t_{YIG} . (b),(c) Time t profile of an input a.c. charge current J_c and output temperature change ΔT for the (b) SPE and (c) Joule heating configurations. (d) An optical microscope image of the sample. The yellow (gray) area above (below) the white dotted line corresponds to the YIG film with ∇t_{YIG} (GGG substrate). \mathbf{H} is an applied magnetic field. (e) An infrared image of the sample. (f) A t_{YIG} profile and cross-sectional image of the sample obtained with a scanning electron microscope.

SPE induces temperature modulation in the Pt/YIG/GGG sample in response to a charge current in the Pt film. When we apply a charge current \mathbf{J}_c to the Pt film as shown in Fig. 1(a), a spin current is generated by the spin Hall effect in Pt [24, 25]. The spin current induces a heat current across the Pt/YIG interface via SPE. The heat current results in a temperature change ΔT which satisfies the following relation [4, 5]: $\Delta T \propto (\mathbf{J}_c \times \mathbf{M}) \cdot \mathbf{n}$, where \mathbf{M} and \mathbf{n} are the magnetization vector of YIG and the normal vector of the Pt/YIG interface plane, respectively. Significantly, the SPE-induced temperature change reflects local t_{YIG} information because the temperature change induced by SPE is localized owing to the formation of dipolar heat sources [5, 7]. Based on the ∇t_{YIG} value and the spatial resolution of our LIT system, we obtained the high t_{YIG} resolution of 92 nm.

The procedure of the LIT-based SPE measurements are as follows [5, 26–31]. To excite SPE, we applied a rectangular a.c. charge current \mathbf{J}_c with the amplitude J_0 , frequency f , and zero offset to the Pt film [Fig. 1(b)]. By extracting the first harmonic response of a temperature change ΔT_{1f}

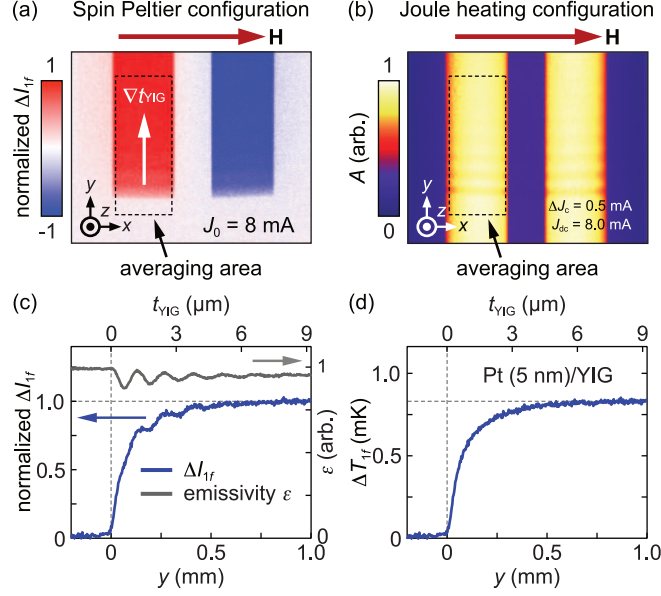


FIG. 2: (a) Lock-in image of an infrared light emission ΔI_{1f} induced by SPE. (b) Lock-in amplitude of the infrared emission A induced by the Joule heating. (c),(d) YIG-thickness t_{YIG} dependence of (c) ΔI_{1f} and the emissivity ϵ and (d) the temperature change ΔT_{1f} induced by SPE.

in this condition (SPE configuration), we can detect the pure SPE signal free from a Joule heating contribution [5, 7]. Here, ΔT_{1f} is defined as the temperature change oscillating in the same phase as \mathbf{J}_c because ΔT generated by SPE follows the \mathbf{J}_c oscillation [Fig. 1(b)] and the out-of-phase signal is negligibly small [5, 7, 32, 33]. In the LIT measurement, we detect the first harmonic component of the infrared light emission ΔI_{1f} caused by ΔT_{1f} , where $\Delta I_{1f} = A \cos \phi$ with A and ϕ respectively being the lock-in amplitude and phase. We converted ΔI_{1f} into ΔT_{1f} by considering spatial distribution of an infrared emissivity ϵ of the sample [5, 7]. All measurements of SPE were performed at room temperature and atmospheric pressure under a magnetic field with a magnitude of 20 mT, where \mathbf{M} aligns along the field direction.

Figure 2(a) shows the ΔI_{1f} image from the Pt/YIG/GGG sample in the SPE configuration with $J_0 = 8$ mA and $f = 5$ Hz. Clear signals appear only on the Pt film with finite t_{YIG} but disappears on the Pt/GGG interface with $t_{\text{YIG}} = 0$ [compare Figs. 1(d) and 2(a)]. The sign of ΔI_{1f} is reversed when \mathbf{J}_c is reversed, which confirms that the observed infrared signal comes from SPE [4, 5]. The spatial profile of ΔI_{1f} along the y direction is plotted in Fig. 2(c), where the ΔI_{1f} values are averaged along the x direction in the area surrounded by the dotted line in Fig. 2(a). ΔI_{1f} gradually increases with small oscillation with increasing t_{YIG} . The oscillation originates from the oscillation

of ϵ of the sample due to multiple reflection and interference of the infrared light in the YIG film [see the infrared light image of the sample in Fig. 1(e)] [7]. To calibrate the ϵ oscillation in the t_{YIG} dependence of SPE, the infrared emission induced by the Joule heating was measured [Fig. 2(b)], where \mathbf{J}_c with the amplitude $\Delta J_c = 0.5$ mA, frequency $f = 5$ Hz, and d.c. offset $J_{\text{dc}} = 8.0$ mA was used as an input for the LIT measurement [Fig. 1(c)] [5]. Since the temperature change induced by the Joule heating is uniform on the Pt film, the lock-in amplitude of the infrared emission A on the Pt film depends only on the ϵ distribution. We found that the obtained t_{YIG} dependence of ϵ ($\propto A$ due to the Joule heating) and the ΔI_{1f} signal due to SPE exhibit the similar oscillating behavior [Fig. 2(c)]. By calibrating ΔI_{1f} by ϵ , we obtained the t_{YIG} dependence of ΔT_{1f} induced by SPE [Fig. 2(d)]. ΔT_{1f} monotonically increases with increasing t_{YIG} . The saturated ΔT_{1f} value for $t_{\text{YIG}} > 6$ μm was determined by using the same Pt/YIG/GGG sample coated with a black-ink infrared emission layer with high emissivity larger than 0.95.

The accurate t_{YIG} dependence of SPE with high t_{YIG} resolution allows us to verify the applicability of several phenomenological models used for discussing the behaviors of SPE. First of all, we found the obtained t_{YIG} dependence of the SPE-induced temperature modulation cannot be explained by a simple exponential approximation [7, 13, 14, 22]. Based on the assumption that the magnon diffuses in YIG with the magnon diffusion length l_m , the simple exponential decay has been used for the analysis of the t_{YIG} dependence:

$$\Delta T \propto 1 - \exp(-t_{\text{YIG}}/l_m). \quad (1)$$

However, in general, this expression cannot be used for the small thickness region since the exponential function should be modulated by the boundary conditions for the spin and heat currents. In fact, the fitting result using Eq. (1) significantly deviates from the experimental data when $t_{\text{YIG}} < 4$ μm (see the green curve in Fig. 3). The observed continuous t_{YIG} dependence of SPE thus requires advanced understanding of the spin-heat conversion phenomena.

Next we focus on two phenomenological models proposed in Refs. 19 and 34. The model in Ref. 19 is based on the linear Boltzmann's theory for magnons and the t_{YIG} dependence of SPE is described as

$$\Delta T \propto \frac{1}{S \coth(t_{\text{YIG}}/l_m) + 1}, \quad (2)$$

where S is a t_{YIG} -independent constant used as a fitting parameter in our analysis. The red curve in Fig. 3 shows the fitting result based on Eq. (2). We found that Eq. (2) shows the best agreement with the experimental result and l_m is estimated to be 3.9 μm . We also analyzed the experimental

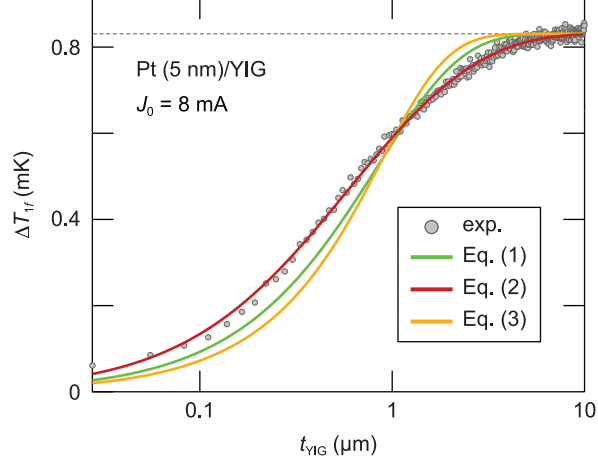


FIG. 3: Experimental results of the t_{YIG} dependence of ΔT_{if} induced by SPE for the Pt/YIG/GGG sample and fitting curves using Eqs. (1)-(3).

results by the model based on the non-equilibrium thermodynamics [34]:

$$\Delta T \propto \frac{\cosh(t_{\text{YIG}}/l_m) - 1}{\sinh(t_{\text{YIG}}/l_m) + r \cosh(t_{\text{YIG}}/l_m)}, \quad (3)$$

where r is a t_{YIG} -independent constant used as a fitting parameter in our analysis. In contrast to Eq. (2), Eq. (3) is less consistent with the experimental results in the whole thickness range (see the yellow curve in Fig. 3) and gives a shorter magnon diffusion length of $0.6 \mu\text{m}$. From the fitting results using Eqs. (1-3), we conclude that Eq. (2) is the best phenomenological model to explain the experimental results on SPE.

To check the reciprocity between SPE and SSE [35], we also measured the t_{YIG} dependence of SSE by using a single Pt/YIG/GGG sample with ∇t_{YIG} . The YIG film used in the SSE measurement was obtained from the same YIG/GGG substrate and the SSE sample was prepared by the same method as that for the SPE sample. The ∇t_{YIG} value of the SSE sample was determined to be $12.2 \mu\text{m}$ per a 1 mm lateral length. To obtain the t_{YIG} dependence of SSE, the SSE signal was measured in the Pt/YIG/GGG sample by means of the thermoelectric imaging technique based on laser heating [23, 36–38]. As shown in Fig. 4(a), the sample surface was irradiated by laser light with the wavelength of $1.3 \mu\text{m}$ and the laser spot diameter of $5.2 \mu\text{m}$ to generate a temperature gradient across the Pt/YIG interface. The local temperature gradient induces a spin current across the interface due to SSE. The spin current is then converted into a charge current via the inverse spin Hall effect in Pt [25]. To avoid the reduction of the spatial resolution of the SSE signal due to the thermal diffusion, we adopted a lock-in technique in the laser SSE measurement, where

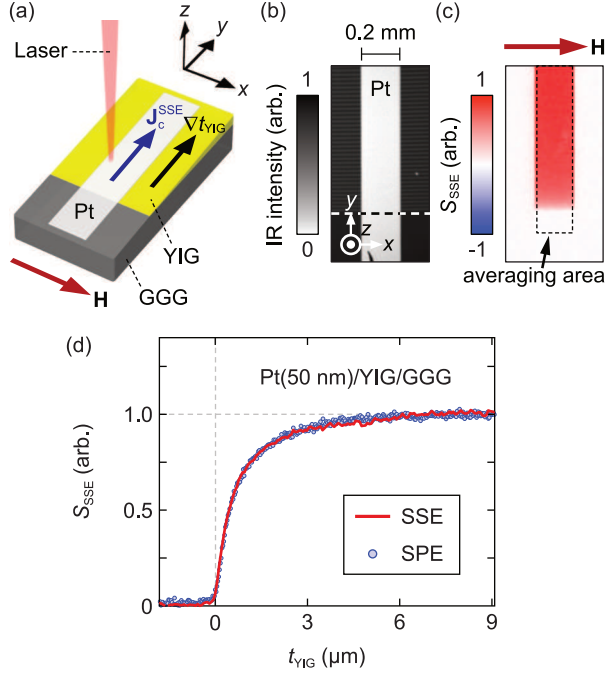


FIG. 4: (a) Schematic of the SSE measurement using a laser heating method. $\mathbf{J}_c^{\text{SSE}}$ is a charge current due to the inverse spin Hall effect induced by SSE. The thickness of the Pt film is 50 nm, which is thick enough to prevent light transmission; the Pt layer is heated by the laser light. (b) Infrared light image of the sample. (c) The SSE signal S_{SSE} image induced by the laser heating. (d) t_{YIG} dependence of S_{SSE} and comparison with that of the temperature change induced by SPE. Here, we used an arbitrary unit for the SSE signal because the temperature gradient induced by the laser heating cannot be estimated experimentally. Nevertheless, the relative change of S_{SSE} is reliable because the heating of the Pt layer is uniform over the sample.

the laser intensity was modulated in a periodic square waveform with the frequency $f = 5$ kHz and the thermopower signal S_{1f} oscillating with the same frequency as that of the input laser was measured. The measurements at the high lock-in frequency realized high spatial resolution for the SSE signal because temperature broadening due to the heat diffusion is suppressed. Here, we defined the SSE signal S_{SSE} as $[S_{1f}(+50 \text{ mT}) - S_{1f}(-50 \text{ mT})] / 2$ to remove magnetic-field-independent background. By scanning the position of the laser spot on the sample, we visualized the spatial distribution of the SSE signal with high t_{YIG} resolution of 64 nm.

Figure 4(c) shows the spatial distribution of S_{SSE} for the Pt/YIG/GGG sample. In response to the laser heating, the clear signal was observed to appear in the Pt film. The t_{YIG} dependence of the SSE signal is plotted in Fig. 4(d), where the S_{SSE} values were averaged along the x direction

in the area surrounded by the dotted line in Fig. 4(c). The SSE signal monotonically increases with increasing t_{YIG} . Significantly, the t_{YIG} dependence of S_{SSE} shows the same behavior as that of the SPE-induced temperature modulation [Fig. 4(d)]. This result supports the reciprocity between SPE and SSE and strengthens our conclusion in the SPE measurement.

In the recent study on SSE in Ref. 21, Parakash *et al.* reported non-monotonical increase of the SSE signal with t_{YIG} . Since the SSE signal takes a local maximum at $t_{\text{YIG}} \sim l_{\text{mp}}$, they estimated l_{mp} as 250 nm from the maximum point. However, in our Pt/YIG samples, the SSE and SPE signals monotonically increase with increasing t_{YIG} . These results suggest that l_{mp} is shorter than the t_{YIG} resolution, 64 nm, in our experiments. The conclusion is consistent with the theoretical expectation of $l_{\text{mp}} \sim 1$ nm [18].

In conclusion, we have discussed the length scale of the spin and heat transport by magnons in YIG by measuring the t_{YIG} dependence of SPE in the Pt/YIG sample. This measurement was realized by using the YIG film with the t_{YIG} gradient and the LIT method, which allow us to obtain the continuous t_{YIG} dependence of SPE in the single Pt/YIG sample. The experimental result is well reproduced by the phenomenological model based on the linear Boltzmann's theory for magnons referenced in Ref. 19 and l_{m} is estimated to be $3.9 \mu\text{m}$ for our YIG sample. We also measured the t_{YIG} dependence of SSE. The SPE and SSE signals show the same behavior in the t_{YIG} dependence and monotonically increase as t_{YIG} increases. The monotonic increase implies that l_{mp} is shorter than 64 nm for our YIG sample. These results give crucial information to understand the microscopic origin of the spin-heat conversion phenomena.

The authors thank R. Iguchi, T. Kikkawa, M. Matsuo, Y. Ohnuma, and G. E. W. Bauer for valuable discussions. This work was supported by CREST "Creation of Innovative Core Technologies for Nano-enabled Thermal Management" (JPMJCR17I1), PRESTO "Phase Interfaces for Highly Efficient Energy Utilization" (JPMJPR12C1), and ERATO "Spin Quantum Rectification Project" (JPMJER1402) from JST, Japan, Grant-in-Aid for Scientific Research (A) (JP15H02012) and Grant-in-Aid for Scientific Research on Innovative Area "Nano Spin Conversion Science" (JP26103005) from JSPS KAKENHI, Japan, the Inter-University Cooperative Research Program of the Institute for Materials Research (17K0005), Tohoku University, and NEC Corporation.

* Electronic address: daimon@ap.t.u-tokyo.ac.jp

† Electronic address: UCHIDA.Kenichi@nims.go.jp

- [1] G. E. W. Bauer, E. Saitoh, and B. J. van Wees, *Nat. Mater.* **11**, 391 (2012).
- [2] S. R. Boona, R. C. Myers, and J. P. Heremans, *Energy Environ. Sci.* **7**, 885 (2014).
- [3] K. Uchida, H. Adachi, T. Ota, H. Nakayama, S. Maekawa, and E. Saitoh, *Appl. Phys. Lett.* **97**, 172505 (2010).
- [4] J. Flipse, F. K. Dejene, D. Wagenaar, G. E. W. Bauer, J. Ben Youssef, and B. J. van Wees, *Phys. Rev. Lett.* **113**, 027601 (2014).
- [5] S. Daimon, R. Iguchi, T. Hioki, E. Saitoh, and K. Uchida, *Nat. Commun.* **7**, 13754 (2016).
- [6] K. Uchida, R. Iguchi, S. Daimon, R. Ramos, A. Anadón, I. Lucas, P. A. Algarabel, L. Morellón, M. H. Aguirre, M. R. Ibarra, and E. Saitoh, *Phys. Rev. B* **95**, 184437 (2017).
- [7] S. Daimon, K. Uchida, R. Iguchi, T. Hioki, and E. Saitoh, *Phys. Rev. B* **96**, 024424 (2017).
- [8] Y. Ohnuma, M. Matsuo, and S. Maekawa, *Phys. Rev. B* **96**, 134412 (2017).
- [9] R. Iguchi, A. Yagmur, Y.-C. Lau, S. Daimon, E. Saitoh, M. Hayashi, and K. Uchida, *Phys. Rev. B* **98**, 014402 (2018).
- [10] K. Uchida, M. Sasaki, Y. Sakuraba, R. Iguchi, S. Daimon, E. Saitoh, and M. Goto, *Sci. Rep.* **8**, 16067 (2018).
- [11] T. Yamazaki, R. Iguchi, T. Ohkubo, H. Nagano, and K. Uchida, *Phys. Rev. B* **101**, 020415(R) (2020).
- [12] T. Kikkawa, K. Uchida, Y. Shiomi, Z. Qiu, D. Hou, D. Tian, H. Nakayama, X.-F. Jin, and E. Saitoh, *Phys. Rev. Lett.* **110**, 067207 (2013).
- [13] T. Kikkawa, K. Uchida, S. Daimon, Z. Qiu, Y. Shiomi, and E. Saitoh, *Phys. Rev. B* **92**, 064413 (2015).
- [14] A. Kehlberger, U. Ritzmann, D. Hinzke, E.-J. Guo, J. Cramer, G. Jakob, M. C. Onbasli, D. H. Kim, C. A. Ross, M. B. Jungfleisch, B. Hillebrands, U. Nowak, and M. Kläui, *Phys. Rev. Lett.* **115**, 096602 (2015).
- [15] R. Itoh, R. Iguchi, S. Daimon, K. Oyanagi, K. Uchida, and E. Saitoh, *Phys. Rev. B* **96**, 184422 (2017).
- [16] S. S.-L. Zhang and S. Zhang, *Phys. Rev. B* **86**, 214424 (2012).
- [17] S. M. Rezende, R. L. Rodríguez-Suárez, R. O. Cunha, A. R. Rodrigues, F. L. A. Machado, G. A. Fonseca Guerra, J. C. Lopez Ortiz, and A. Azevedo, *Phys. Rev. B* **89**, 014416 (2014).
- [18] L. J. Cornelissen, K. J. H. Peters, G. E. W. Bauer, R. A. Duine, and B. J. van Wees, *Phys. Rev. B* **94**, 014412 (2016).
- [19] S. S. Costa and L. C. Sampaio, *J. Phys. D: Appl. Phys.* **53**, 355001 (2020).
- [20] B. Flebus, S. A. Bender, Y. Tserkovnyak, and R. A. Duine, *Phys. Rev. Lett.* **116**, 117201 (2016).
- [21] A. Prakash, B. Flebus, J. Brangham, F. Yang, Y. Tserkovnyak, and J. P. Heremans, *Phys. Rev. B* **97**,

- 020408(R) (2018).
- [22] E.-J. Guo, J. Cramer, A. Kehlberger, C. A. Ferguson, D. A. MacLaren, G. Jakob, and M. Kläui, *Phys. Rev. X* **6**, 031012 (2016).
- [23] R. Iguchi, S. Kasai, K. Koshikawa, N. Chinone, S. Suzuki, and K. Uchida, *Sci. Rep.* **9**, 18443 (2019).
- [24] A. Hoffmann, *IEEE Trans. Magn.* **49**, 5172 (2013).
- [25] J. Sinova, S. O. Valenzuela, J. Wunderlich, C. H. Back, and T. Jungwirth, *Rev. Mod. Phys.* **87**, 1213 (2015).
- [26] H. Straube, J.-M. Wagner, and O. Breitenstein, *Appl. Phys. Lett.* **95**, 052107 (2009).
- [27] O. Breitenstein, W. Warta, and M. Langenkamp, *Lock-in Thermography: Basics and Use for Evaluating Electronic Devices and Materials* (Springer Science & Business Media, 2010).
- [28] O. Wid, J. Bauer, A. Müller, O. Breitenstein, S. S. P. Parkin, and G. Schmidt, *Sci. Rep.* **6**, 28233 (2016).
- [29] O. Wid, J. Bauer, A. Müller, O. Breitenstein, S. S. P. Parkin, and G. Schmidt, *J. Phys. D: Appl. Phys.* **50**, 134001 (2017).
- [30] T. Seki, R. Iguchi, K. Takanashi, and K. Uchida, *Appl. Phys. Lett.* **112**, 152403 (2018).
- [31] K. Uchida, S. Daimon, R. Iguchi, and E. Saitoh, *Nature* **558**, 95-99 (2018).
- [32] R. Iguchi and K. Uchida, *Jpn. J. Appl. Phys.* **57**, 0902B6 (2018).
- [33] A. Yagmur, R. Iguchi, S. Geprägs, A. Erb, S. Daimon, E. Saitoh, R. Gross, and K. Uchida, *J. Phys. D* **51**, 194002 (2018).
- [34] V. Basso, E. Ferraro, A. Magni, A. Sola, M. Kuepferling, and M. Pasquale, *Phys. Rev. B* **93**, 184421 (2016).
- [35] A. Sola, V. Basso, M. Kuepferling, C. Dubs, and M. Pasquale, *Sci. Rep.* **9**, 2047 (2019).
- [36] M. Weiler, M. Althammer, F. D. Czeschka, H. Huebl, M. S. Wagner, M. Opel, I. M. Imort, G. Reiss, A. Thomas, R. Gross, and S. T. B. Goennenwein, *Phys. Rev. Lett.* **108**, 106602 (2012).
- [37] N. Roschewsky, M. Schreier, A. Kamra, F. Schade, K. Ganzhorn, S. Meyer, H. Huebl, S. Geprägs, R. Gross, and S. T. B. Goennenwein, *Appl. Phys. Lett.* **104**, 202410 (2014).
- [38] J. M. Bartell, C. L. Jermain, S. V. Aradhya, J. T. Brangham, F. Yang, D. C. Ralph, and G. D. Fuchs, *Phys. Rev. Appl.* **7**, 044004 (2017).